communications physics

Article

https://doi.org/10.1038/s42005-024-01745-z

Life and death of a thin liquid film

Muhammad Rizwanur Rahman [1] ✉, Li Shen[1], James P. Ewen[1], David M. Heyes[1], Daniele Dini [1] & Edward R. Smith[2]

Thin films, bubbles and membranes are central to numerous natural and engineering processes, i.e., in solar cells, coatings, biosensors, foams, and emulsions. Yet, the characterization and understanding of their rupture is limited by the scarcity of atomic detail. We present here the complete life-cycle of freely suspended films using non-equilibrium molecular dynamics simulations of a simple atomic fluid free of surfactants and surface impurities, thus isolating the fundamental rupture mechanisms. We identified a short-term 'memory' by rewinding in time from a rupture event, extracting deterministic behaviors from apparent stochasticity. A comprehensive investigation of the key rupture-stages including both unrestrained and frustrated propagation is made—characterization of the latter leads to a first-order correction to the classical film-retraction theory. The highly resolved time window reveals that the different modes of the morphological development, typically characterized as nucleation and spinodal rupture, continuously evolve seamlessly with time from one into the other.

Isaac Asimov's *Foundation* series introduced the concept of *psychohistory* - where historical trends enable statistical forecasts of the overall trajectories of the civilization while not predicting individual or transient events. This parallels the well known notion from statistical physics of being microscopically stochastic yet macroscopically deterministic—an important distinction as we work through a complete description of the multi-scale rupture process of a thin liquid film.

The stability and rupture of thin films hold vast significance in a wide spectrum of applications[1,2], ranging from natural processes like gravity currents, lava flows, and snow avalanches[3,4] to biological transport processes in lungs and cell membranes, and in disease transmission and forensic analyses[5–7], to more common place engineering applications in miniaturized micro-electronic, micro-fluidic and biomedical devices[8,9], complex coatings, distillations and insulation[10,11] - to name a few. Consequentially, the literature concerning the stability and rupture of thin liquid films is voluminous - encompassing theoretical[12–16], experimental[17–19], and numerical[20–24] investigations. The rupture process, in general, is associated with an activation energy of $\mathcal{O}(\gamma h^2)$[25], where h and γ denotes, respectively, the thickness and the surface tension of a film. Although this renders this mechanism improbable for thick films[26], the probability of rupture increases as thickness decreases, and becomes most significant for films thinner than *ca.* 10 nm. The spontaneity in the rupture process is mostly triggered by the growth of fluctuations, and corrugations of the surface due to thermal motion that weakens the film, leading to rupture. These undulations assume increasing importance for films with nanoscopic thickness, as highlighted by the molecular dynamics (MD) investigation of Zhang et al.[27], and reduce the critical wavelength causing rupture.

In addition to the continuous distortion of the liquid-vapor interface due to thermal fluctuations[28], spatial variations of surface tension[29] induces fluid movement, though it tends to be overlooked in the majority of theoretical models. The considerations of uniform thickness and a stationary interface, as in the study of Derjaguin and Prokhorov[14], result in a rupture thickness within the range of a few hundred nanometers. In contrast, Anderson et al.[30] conducted a linear stability analysis of thinning films, showing that rupture actually occurs when the film thins down to a few tens of nanometers. Yet, the linear theories cannot follow the film evolution until rupture since their validity ceases as the disturbances in the film grow sufficiently. Inclusion of the non-linear terms showed that any local thinning of a free standing film amplifies the influence of the long-range force, accelerates film rupture[31,32] while simultaneously attenuating the effects of surface tension[33]. The importance of relaxing the linear approximations in the film stability and rupture studies is further realized by the fact that the non-linear theory yields significantly shorter times of rupture from those obtained through the linear models, as much as an order of magnitude[33].

While the impressive body of research outlines the complexities of rupture dynamics for free standing non-draining films - which are of significance for numerous colloidal systems, from coalescence of emulsions to fusion of lipid bi-layers, and for biological membranes[34,35], the literature also underscores the crucial role, as well as the ambiguities of the contact line properties in rupture behavior for supported films. A method that reduces these ambiguities involves eliminating the solid-substrate[36,37]. Replacing the solid with a liquid substrate cures any contact line singularity at the interface, and exhibits distinct dewetting behavior[38]. Regardless, it introduces a nuanced dependency on the properties of the liquid-liquid interface.

[1]Department of Mechanical Engineering, Imperial College London, South Kensington Campus, London, UK. [2]Department of Mechanical and Aerospace Engineering, Brunel University London, London, UK. ✉e-mail: m.rahman20@imperial.ac.uk

An unbounded film (as in foams and bubbles), in this context, removes interference from any substrate, whether liquid or solid, and thereby can serve as a reference point of rupture dynamics. However, the presence of two free surfaces, the undulations therein, and the complexity which predominantly resides in the spatio-temporal dynamics of the liquid-vapor surface contributed to the lack of clarity in our understanding of the origin, and the unfolding of the rupture process.

For the break up of thin films, local fluctuations in film density and thermal noise have non-negligible impact[39,40], and depending on the scale of the problem they may stabilize or de-stabilize the film[41]. By manipulating the ratio of hydrodynamic to capillary stresses in polymer solution films, Chatzigiannakis and Vermant[42] demonstrated the increasing dominance of (stochastic) thickness fluctuations over the (deterministic) hydrodynamic forces. The impact of these atomic scale local fluctuations, leading to the ultimate failure of a thin film, constitutes the key focus of this study. We choose a homogeneous system composed of pure Lennard-Jones particles - thereby, focusing on the fundamental physical response of the film. These films, while relevant to the rupture of surfactant-free metallic films[30,43], liquid crystals[44], emulsions and membranes[35], and for films in micro-gravity environment[45], also enhances the general understanding of the importance of atomic-scale local fluctuations in rupture mechanism.

Notably, despite the morphological similarities with surfactant laden and supported films, free standing pure films exhibit fundamental differences. Consequently, the insights obtained, while illuminating, may not be directly applicable to the former cases due to the necessity of considering surfactant properties, contact line dynamics, gradient-driven advection, and diffusion. The intricate coupling among these processes has rendered their direct measurements elusive. Furthermore, any effort to trace contaminants invariably modifies their properties, thereby effecting the system's dynamics[46]. In contrast, with direct access to individual molecules and their immediate properties, our MD investigation of pure films establishes a reference-point for studies addressing more complex and specific scenarios.

The central topic of the current investigation concerns the complete life-span of thin (black) films, and their rupture mechanism. By presenting the fundamental aspects and the behavior of thin films at the smallest of scales, and mapping the mechanisms responsible for the evolution of films across space-time coordinates, we provide a simplified, yet fundamental view of the evolution of thin-film dynamics. This is achieved by tracing back and explaining the links between inception and fragmentation phases, and by identifying the similarities emerging at different scales. The subsequent sections of this manuscript are structured as follows: we begin by identifying the shared characteristics among various modes of rupture, and unify them. Following this, we demonstrate a time-sequencing behavior of the film in the moments leading up to its rupture. The deterministic aspect within the typically stochastic rupture process—which is quantitatively identified for the specific case of liquid film in this study—underscores the general principle that the stochastic-to-deterministic transition is a common thread across diverse fields of study. Finally, we provide detailed illustrations of the nucleation/rupture event, and the late stage frustrated propagation leading to coalescence. The latter highlights the factors responsible for slower propagation and, hence, delayed coalescence. To avoid any potential ambiguity, we emphasize that by the term 'nucleation' we exclusively refer to the atomistic process of hole formation in the freely suspended films, characterized by diffused interfaces.

Results and discussions

The rupture process is long preceded by the drainage and subsequent thinning of the metastable film. Thinning is driven by capillary suction, which is followed by the development of an instability leading to rupture. Such an instability is caused by the heterogeneity in film thickness, or due to the gradients in surface concentration[47,48]. Figure 1 summarizes the full lifetime of a film: starting from hydrodynamic thinning at micron thickness (region 1 in Fig. 1) and fluctuations dominated thinning at nanoscale (region 2), followed by a piercing stage when surface fluctuations grow more rapidly at some sites (or, locations) compared to others leading to nucleation (region 3). Depending on the initial film thickness, however, the rupture process may follow one of the several modes; and although a stochastic process, a finite window of memory is observed - these we discuss in the next two sections. Once the film is punctured, a short term exponential growth regime emerges (region 4, also see Supplementary Fig. 7) when the nucleus attains a circular shape and eventually enters the linear growth regime (region 5). This linear growth, referred to as the Taylor-Culick retraction, has been extensively investigated in the literature, both numerically and by experiment; and has been studied for freely suspended Lennard-Jones (LJ) films in an earlier study by the authors[49], also through MD simulations as here. It was observed[49] that by appropriately resolving the surface forces, curvature effects, and the momentum of the accumulated liquid mass, the Taylor-Culick framework, which was originally proposed[50,51] and examined[52] for soap films and films with surfactants, is highly effective at describing the retraction of atomic-scale pure unbounded films. Depending on the modes of rupture and the film thickness, multiple rupture sites may nucleate and continue to grow. This growth is later affected by the presence and growth of neighboring nuclei, and a frustrated growth regime emerges (region 6) leading to delayed coalescence and coarsening.

Modes of rupture

Spinodal rupture vs. nucleation. In a freely suspended film (and also those on a substrate), *spinodal process*[26,53–56] refers to its solely thermodynamic and rapidly spontaneous disintegration under the influence of molecular interactions. For films with surface impurities or defects, the energy barrier that the film needs to overcome in order to nucleate is (locally) lowered resulting in *nucleation* randomly distributed over the film. In the absence of surface defects and contaminants, as in the present study, nucleation-like events can still occur as a result of (thermal) fluctuations. The occurrence of surface instability is primarily connected to linearly unstable films, and nucleation at defects is often linked to metastable films; Thiele et al.[55], yet showed instability dominated and nucleation dominated sub-ranges within the linearly unstable range. Through non-linear Cahn-Hilliard framework Novick-Cohen[57] reported a smooth transition in the phase separation dynamics. Present results give evidence of the co-existence of spinodal-like and the nucleation-like modes of rupture in freely suspended thin films. Figure 2 shows snapshots of the film thickness at different times for varying initial thickness, h_0. Note, unless otherwise stated, all parameters are reported in Lennard-Jones units, i.e., length in σ where $\sigma = 0.34$ nm. The thinnest film ($h_0 \sim 8.5$, top row) displays transition from 'vapor-in-liquid' to bi-continuous to 'liquid-in-vapor' state commonly seen in spinodal process[58]. The irregular shapes and sizes of the nuclei arise not only from early coalescence but also from the interactions between, and coalescence of, neighboring nuclei. As the film thickness increases (from top to bottom panels), the nuclei become more circular, and regularly shaped – a typical characteristic assigned to nucleation[59–61].

The coexistence of both of the modes discussed above was also observed for evaporating structural protein films[61], for liquid metals[44,62,63], and for polymer films[53,64,65]. However, these studies were based on liquid films on solid substrates, and to the best of our knowledge, the rupture of freely suspended single component films has not been systematically investigated until now. In the current study, the observations of rupture for various thicknesses agree qualitatively with the commonly observed patterns found for spinodal and nucleation-like rupture; but most importantly, these are found to initiate spontaneously without the presence of surface impurities or external perturbations. It is clear from the present free film model that the nucleation observed in this study must arise from highly localized thermal fluctuations, in contrast to any substrate defect as in Thiele et al.[61] and elsewhere.

The identification of the predominant mechanism and their potential overlapping has been a focal point of research for years[44,55,61]. A critical and intuitive determinant is the modality of the hole size distributions[61]. In the present study, we observe that thicker films displays unimodality, typically assigned to nucleation, whereas, relatively thinner films predominantly

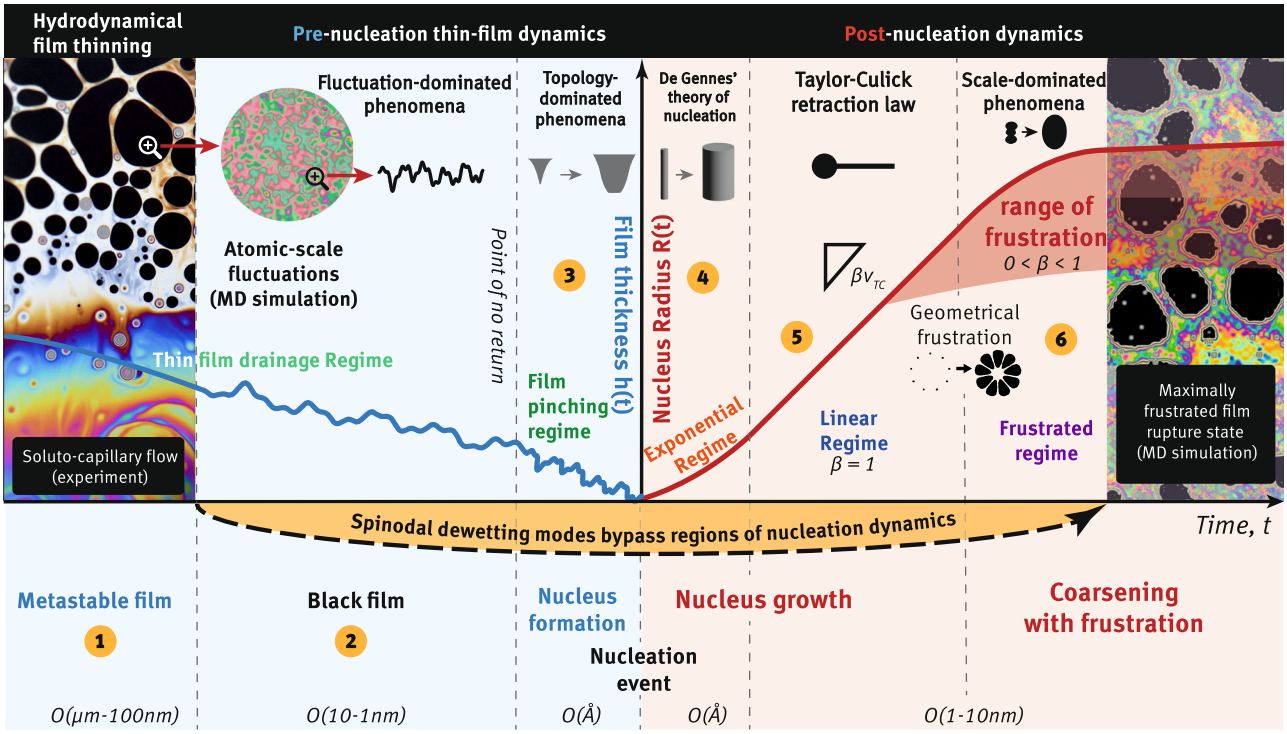

Fig. 1 | Portrait of the life-span of a thin-film. The left half of the schematic, regions 1–3, shows thinning in stages before hole formation, the y-axis represents film thickness (not to scale). The far-left (region-1) snapshot shows (experimental) hydrodynamic thinning in a micron-thickness metastable film which leads to the formation of nanoscopic black films. Remaining parts of the schematic summarizes molecular dynamics observations which are inaccessible by experimental investigation: (region-2) fluctuation dominated thinning of black films, (region-3) as rupture becomes imminent, thinning is accelerated and leads to film pinching (when a particular site overcomes the nucleation-state) and eventually to nucleation when $h = 0$. The just-nucleated site now starts expanding. Subsequent growth of the ruptured site is presented in the right half of the figure (shaded in faint red, regions 4–6) with the y-axis now representing the radius of the rupture site. (region-4) Initially growth is exponential which soon attains (region-5) linear growth. As more sites rupture across the film, their presence and mutual growth frustrates the growth of any individual site as in (region-6) which later follows coalescence and coarsening - the far right snapshot from MD simulations shows a typical state of the (black) film at this stage with expanding holes in it. The spinodal rupture is fast-forwarded from 1 to 6, even at the MD scale, (almost) bypassing the intermediate stages.

exhibits bimodal distribution, indicative of the existence of two distinct hole formation mechanisms[53,61,62]. These observations, detailed in the Supplementary Information (Supplementary Fig. 12 showing size distributions for films with $h_0 \sim 11$ vs. 9.5, and associated discussions), underscore the nuanced interplay between film thickness and rupture behavior.

Upon the formation of a nucleus within a comparatively thicker film, it undergoes expansion at the Taylor-Culick speed, creating a rim (where the liquid accumulates) encircling it[49]. This rim serves as a deterrent to the growth and coalescence of approaching neighbor nuclei, and thereby delays coalescence (which we discuss later in further detail). When an individual nucleus finds it energetically more favorable to amalgamate than to continue to grow, coalescence takes place. In contrast, the dynamics differ for spinodal rupture where holes appear 'almost' simultaneously at multiple sites, creating a uniform distribution across the film. Consequently, the nuclei face spatial constraints, hindering their expansion. Additionally, spinodal rupture typically takes place in relatively thinner films with higher nuclei growth rates, facilitating easy expulsion of the liquid bridge trapped between neighboring nuclei resulting in an earlier coalescence stage.

Notably, these observations highlight that the overlapping of, and the transition between these modes can occur solely based on the thickness of the film, and on the spread of the surface instability, indicating the critical role played by the film thickness in determining the dominant mechanism. This, therefore, expands the remit of the present results potentially to other substrate-free situations. In addition, it can be inferred that any apparent dissimilarity in the rupture patterns of two films of different h_0 must arise from the spatio-temporal distribution of the rupture events. If these differences are removed, one obtains similar evolution across scales - from growth to fragmentation (see Supplementary Note 1: Nuclei Growth, for further details). This is also reminiscent of the work of Nguyen et al.[44], who studied the early stages of rupture in nanometer-thick liquid-metal films. Their MD simulations reveal that spinodal instability and nucleation mechanisms simultaneously occur within these films. Thus our results indicate that these macroscopically different processes originate from a shared molecular basis.

Memory of rupture

The probabilistic nature of film rupture process prohibits any precise prediction of the time and location of a rupture event, especially for a defect free surface. We observed a short-term window before the rupture event where it becomes deterministic - even with a perturbation applied to the trajectories. This allows us to link this observation to the concept of the transition from microscopic stochasticity to macroscopic determinism. For the rupture of thin liquid films, this is the state where the first hole will nucleate in a specific bounded region Ω of space, almost surely, regardless of the number of times the scenario is repeated whereby each individual repetition produces a slight alternation of the trajectory of film evolution. In Fig. 3, Ω is schematically represented by the circular rupture spot. Moreover there exists a brief time-window, Σ, shown in Fig. 3 as the rupture memory region, within which we can rewind the film state and still achieve rupture in Ω. Together, the region defined by $\Omega \times \Sigma$ forms the spatio-temporal boundary for the stochastic-to-deterministic transition characteristics of a film approaching its first rupture event.

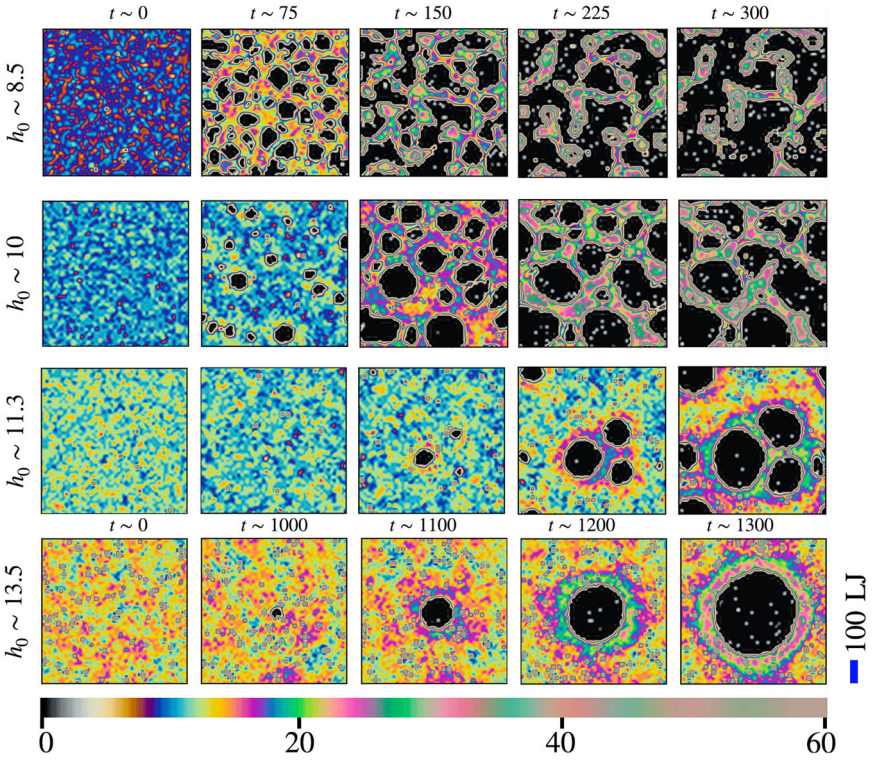

Fig. 2 | Spontaneous rupture of films of different initial thicknesses. From top to bottom, $h_0 = 8.5$, 10, 11.3 and 13.5 in LJ units. Color maps represent the local thickness, bar at the lower right shows length scale in Lennard-Jones units. The presence of surface modulations are seen in the unruptured states of the films.

To explore this temporal duration of the impending rupture events, we systematically preserved the system's state at regular intervals and subsequently resumed the simulation from those instances onward, see *Materials and Methods*. Repetition of these computer experiments, with different phase-space trajectories, highlights the inherent weak extent of 'memory' in the film-rupture process. This means that, under identical initial conditions, the time and location of rupture exhibit variability in independent simulations, except for an exceptionally narrow time interval during which the film displays deterministic behavior. Figure 3 elucidates this dynamics. The top plot illustrates density fluctuations over time, with filled red symbols representing the local density at the center of a rupture site that nucleates at $t \sim 580$. The cyan curves portray local density at all other film positions, showcasing temporal fluctuations through the curve bandwidth. Throughout this extensive time span, despite the density of the rupture site closely following the lower boundary of the density spectrum, no abnormal deviations relative to other density profiles occur. Hence, assigning a critical lower density threshold would be inaccurate. This is supported by the observation of the density profiles at certain regions that do indeed experience significant density reduction (see the cyan density profile that approaches $\rho < 0.2$ at $t \sim 520$), they do not culminate in rupture/nucleation events.

The time instances denoted by the orange or blue circles on the density plot (and, also on the time-axis encircling the black circles) mark the moments when independent simulations were re-started. These instances are reproduced, alongside the time axis, in the lower panel, where the $y - z$ coordinates of the film are depicted, pinpointing rupture sites represented by filled circles. Connection lines link each restart time to its corresponding rupture location. The larger black circle designates the rupture site of the original trajectory ($t_n \sim 580$, as displayed in the top panel's). Notably, in a simulation recommenced from an earlier state, i.e., $t_0 \sim 520$, the film still nucleated at the same spot. This consistent location remained unaltered until $t_0 > 481$. The case (re)started from $t_0 \sim 481$ is particularly important as one can identify a rise in the local density which implies that a relatively thicker area on the film can be more prone to rupture than a thinner area. To corroborate this observation, multiple independent simulations were conducted around $t_0 \sim 481$. Even when introducing minor perturbations to the initial trajectory, the film consistently underwent rupture at the identical site. Restarting the simulation from a state earlier than ~ 480 introduced a distinct behavior, where the film undergoes rupture at random and diverse locations and times. These stochastic rupture sites are depicted as faint red circles in the figure, linked by blue lines to corresponding restart times. Among these latter cases, when restarting from the state at $t_0 \sim 449$, one of the cases coincidentally nucleated at the same location as the original simulation, which we regard as an incidental occurrence. A similar rewind is conducted for another case for which $t_n \sim 450$, see Supplementary Fig. 4, the film is observed to nucleate at a different location and at a different time, but exhibits similar characteristics with a different spatio-temporal boundary - suggesting reduced, if not complete absence of, stochasticity[42] within the memory-window. In particular, this window is an indication of the intrinsic non-linearity associated with rupture.

In contrast to fluctuating hydrodynamics which introduces a random forcing term to model the probabilistic nature of nano-scale fluctuations, MD simulations have apparent stochasticity due to the complexity of interpreting evolution of the full 6N dimensional phase space. Yet, our study reveals a striking observation: holes consistently form at the same locations across simulations, provided we restart within the rupture memory window. This spatial consistency in hole formation, despite different phase-space trajectories and apparent stochasticity, complements and extends the insights from prior studies[66,67]. As illustrated above, local density alone cannot define the likelihood of rupture. The local energetic profiles at the rupture site can be approximated as[1,26] $U = \int\int (\frac{\gamma}{2}|\nabla h|^2 - \frac{A}{4\pi h^4}(h - h_0)^2)\, dx\, dy$, where γ and A are, respectively, the surface tension of film liquid, and the Hamaker constant, h is the film thickness, h_0 is initial thickness. The local energetics with fluctuating hydrodynamics have been successful in predicting the onset of thermal rupture, the readers are referred to recent works of Sprittles et al.[67,68], and the references therein. Although the deterministic rupture in the memory window did not seem to be trivially predictable by these local energies (see Supplementary Fig. 3 and associated discussions), the existence of a saddle point and a surrounding basin of attraction in the energy landscape might be valid starting point to understand rupture memory, perhaps requiring a non-linear stochastic model.

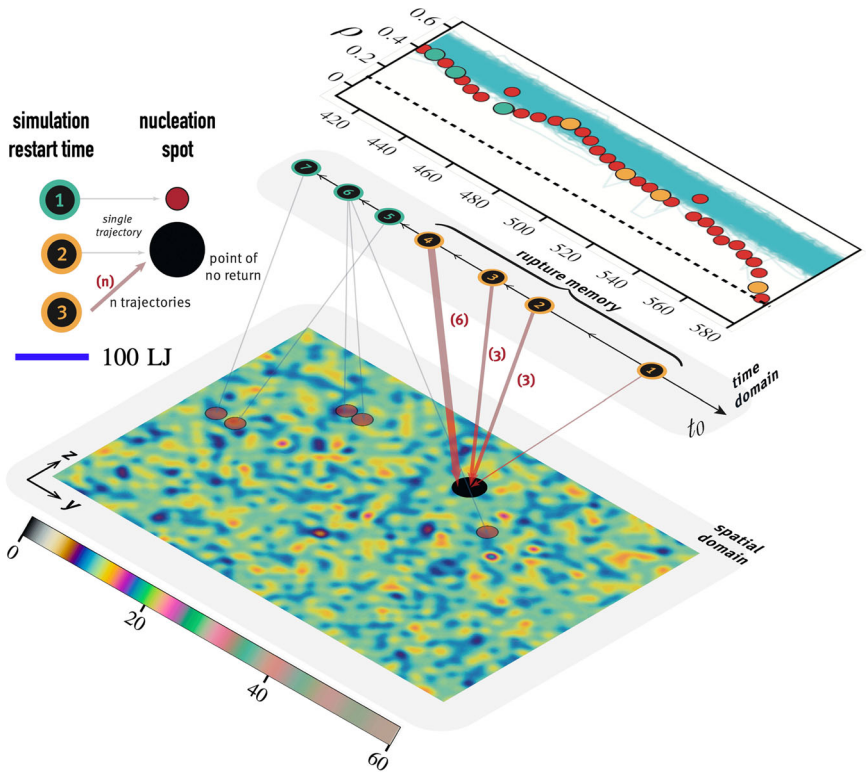

Fig. 3 | Memory of rupture. Temporal variation of the thickness-averaged local density. The circles corresponds to density of a location where nucleation occurs at $t \sim 580$, whereas, the cyan curves shows local density at other locations on the film which do not nucleate within the time plotted here. Several independent simulation were restarted at time $t = 418, 449, 481, 504, 520, 571$ - these time instances are marked by the circles on the time axis, and the corresponding density of the ruptured site at those time instants are marked by blue and orange circles. On the colormap which shows a snapshot of the film, the position of nucleation for every case is depicted either by a black circle if the location of nucleation remains the same as of the original case, or by a red circle if the film nucleates at a different location. Similarly, red lines connect nuclei when films nucleate at the same spot as the mother film, and blue lines connect otherwise. (n) shows number of independent simulations (also represented by thickness of the connecting lines), omitted if $n = 1$. Bar shows length scale in Lennard-Jones units.

A plausible interpretation of the probabilistic to the deterministic transition can be framed in terms of Stillinger's inherent structure theory of dynamical evolution in liquids, which has been widely applied to many aspects of liquid dynamical phenomena at the molecular level[69–72]. In this theory it is proposed there is a so-called 'basin of attraction' formed from all those equilibrium molecular configurations - which when quenched, instantaneously collapse into the *same* underlying or 'inherent' structure, some of which we have seen are precursors to nucleus formation. This is evidence of the non-classical form of rupture which suggests more complex pathways of hole formation that involves intermediate stages[73]. The trajectories (re)started from different points in time, despite their microscopic randomness, are perhaps still attached to the same inherent structure and results in the same outcome. If one goes too far back in time, slight differences in the trajectory associated with the restart may cause the system to evolve in a way where it becomes associated with or 'captured' by another inherent structure which may not lead to a nucleus (unlike the situation before the rewind). In the present context, certain inherent structures can be viewed as acting as 'gateways' to hole formation. The residence time for these inherent structures is at least ~ 100 Lennard-Jones time units[74], aligning with the observed duration of the memory window in this study, which underscores the necessity of a full atomic model to capture the memory effect.

Formation, frustration and coalescence

The time of nucleation (or, rupture) inherently possesses a probabilistic nature[75], and is subject to fluctuations determined by thermodynamics and other influencing factors. Based on the underlying assumptions, the theoretical prediction of rupture time for free films with thickness h, in the absence of surfactants or any surface impurities, scales as[76,77] $\tau \sim h^3$, we discuss these literature in greater details in Supplementary Note 3: Formation of a Nucleus, and compare with the results from current investigation over a range of film thickness. Regardless of the time of rupture (and hence the initial thickness of the film), spontaneous rupture process is preceded by localized thinning, and all rupture sites inevitably undergo the fluctuations dominated thinning phase - which is noticeably accelerated as the film approaches the rupture event (schematically shown in region 3 of Fig. 1, quantitative details in Supplementary Note 3). Once a film nucleates in our simulations, the highly resolved space-time allow to trace back to the immediate proximity of the rupture event to capture the formation phase of the hole (i.e., nucleus). The radial averaged local density profile of the center of a nucleus is reconstructed in Fig. 4a where the initiation of local thinning is evident ahead of the rupture, i.e., at $t_{n-2\delta t}$, where $\delta = 25$. Upon the film's substantial perforation and the subsequent formation of a rim encircling the nucleus, expansion ensues through exponential, and linear growth rates.

The growth of an isolated nucleus is well understood through the seminal works of Taylor and Culick[51,78] and subsequent detailed studies[52,79–81]. However, a more commonplace observation is that of a film with multiple rupture sites requiring the considerations of their collective interactions and growth[62,63]. The absence of neighbors, or equivalently the consideration of infinite liquid films[81,82] does not account for any interaction between propagating rupture sites, and is only realized when the edge effect is accounted for[83]. If one considers two neighboring nuclei on a film, these may exhibit three distinct types of behavior in stages: (i) individual uninterrupted growth until when the nuclei come to close proximity of each other, (ii) disturbed growth due to the presence of the neighbor leading to (iii) delayed coalescence. The first stage is predominantly governed by surface tension dynamics. At the second stage, surface tension favors the growth of the nuclei, but coarsening of the bridge between the neighbors retards growth. The third stage requires drainage of the liquid bridge, followed by subsequent thinning and rupture.

The thickness of this liquid bridge between two neighboring nuclei is notably greater if the nuclei have undergone sufficient growth over time before coming close to each other. This arises because the liquid particles from the nuclei accumulate in the surrounding rim, forming a barrier that impedes merging. (Refer to the Supplementary Note 4: Neighbor Effect on the Rupture Propagation, for a scenario where a larger nucleus opts to displace a relatively smaller nucleus rather than coalescing with it.) However, there are situations where nuclei have expanded extensively and multiplied to the extent that they encounter space limitations, compelling coalescence as the sole energetically favorable course of action to continue to

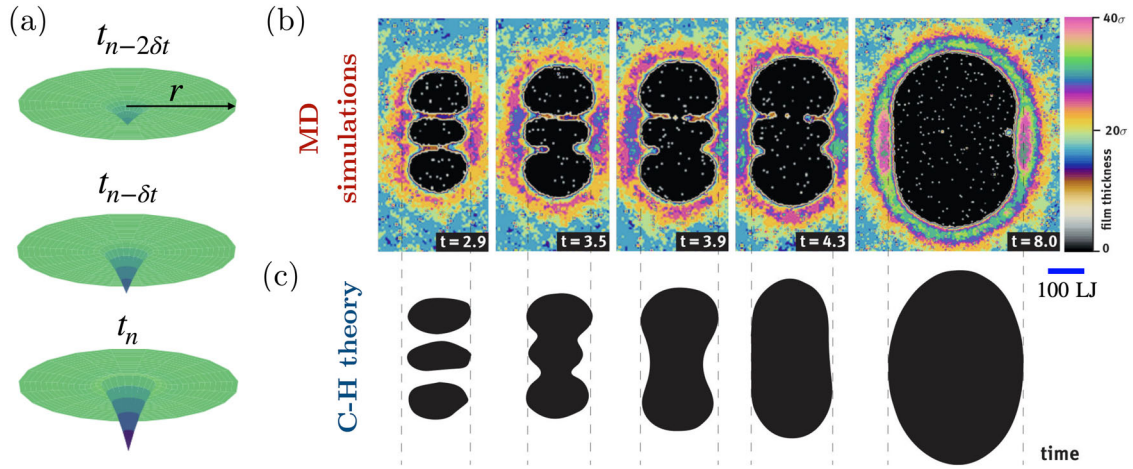

Fig. 4 | Formation and coalescence of rupture sites. a Formation of a nucleus: radial averaged density profile around a rupture site at times closer to its nucleation is revolved around the center to reconstruct the rupture process, $h_0 \sim 11.2$, $r = 0$ is the center of the nucleus, and $\delta t = 25$ units of MD time. Coalescence of nuclei: (**b**) MD simulations; (**c**) Finite Element Analysis using the phenomenological Cahn-Hilliard theory, color maps denote local thickness, bar shows length scale in Lennard-Jones units. Both panels are reminiscent of the experimental study of Dolganov et al.[98] using free-standing smectic films.

evolve. This phenomenon is illustrated in Fig. 4, where the panel (b) showcases results from MD simulations depicting the temporal evolution of three artificially generated nuclei, capturing their initial growth, coalescence, and subsequent expansion beyond coalescence.

Following the onset of the rupture of the film, the system essentially enters a state that can be considered over damped, and one may use the thickness data with the nuclei already formed (from MD) as an initial condition for Cahn-Hilliard (C-H) theory. Correspondingly, Fig. 4c depicts analogous outcomes derived from finite element analysis utilizing C-H theory (see Methods, and Supplementary Note 6: Cahn-Hilliard Theory). Notably, coalescence commences only when the nuclei encounter constraints impeding further expansion. This qualitative analogy between the outcomes of the two different methods, i.e., MD vs. C-H simulations, indicates the scale invariance of coarsening despite their potentially different underlying physics.

Figure 5a shows the time-evolution of the radii of three synthetic nuclei (by 'synthetic' we mean non-spontaneous nucleus which was induced by applying an exponential force—mimicking the poking of a film in experimental studies[81,84] – in an otherwise stable film, see: methodology) before and beyond coalescence (few representative snapshots are shown in panel e). Initially the nuclei are distant from each other and a very short term exponential growth (see Supplementary Fig. 7) is followed by the Taylor-Culick linear regime[49,81]. However, and as depicted by the red line, the growth of the central nucleus (n_2) is affected by the presence of the two expanding side-nuclei (n_1, n_3) until it coalesces with one of them. Beyond coalescence, the combined nucleus (n_1 and n_2) maintains linear growth. It is observed from the slopes of the blue (single nucleus, n_3) and the black (coalesced n_1, n_2, i.e., $n_{c,1,2}$) lines, that the growth rate of the single nucleus, n_3 and that of the coalesced nucleus, $n_{c,1,2}$ are equal. However, after the final coalescence at around $t/\tau \sim 4$, a slightly steeper slope (of the black line, $n_{c,1,2,3}$) is observed, this is because the growth is no longer restrained by any surrounding nucleus and there is sufficient space for expansion (the film is larger in lateral dimension than in panel e which shows only the area surrounding the nuclei). Notably, the dashed line denotes the equivalent radial growth of the three nuclei ($R_{eq} = \sqrt{A/\pi}$, with $A = \sum_{i=1}^{3} A_i$) which as well, captures the growth rate of the coalesced nuclei, and thus proves to be a representative measure. More importantly, and in agreement with previous conclusions[63,64], this implies that the growth of a coalesced nucleus can be extrapolated to the initial nucleation time, provided that growth is hindrance free. Jacobs et al.[64] carried out a similar extrapolation in time for an estimation of the rupture time, but without considering any temporal behavior of the nucleus distribution in spinodal process, and any dynamical instability thereof. Herminghaus et al.[63] also proposed the use of nucleus diameter as a 'clock' for the rupture. However, we will shortly see that such a straightforward extrapolation in time is valid only for a few special cases, and generally imprecise, if not prohibitive.

Figure 5b provides insight into the growth dynamics of the equivalent nucleus radius, R_{eq}/h_0 (depicted as red circles corresponding to the left y-axis), and the number of nuclei (illustrated as blue circles corresponding to the right y-axis) for a relatively thinner film ($h_0 \sim 10$) that ruptures spontaneously; panel (f) presents representative snapshots of this process. In panel (b), the reference point $t/\tau_i = 0$ denotes the time of the first nucleation event. The number of nuclei (blue circles) initially rises during the nucleation phase and subsequently declines from $t/\tau_i \sim 5.8$, indicating the transition to the coalescence regime. The red circles trace the time evolution of the equivalent nucleus radius, revealing a linear growth during the nucleation regime, followed by a phase of quasi-stagnation where R_{eq} experiences marginal increments. This contrasts with the observations in panel (a) where the growth rate increased after coalescence. The underlying reason for this divergence in growth patterns lies in the available space for expansion. For the case in panel (a), the coalesced nuclei have sufficient room to expand, as exemplified by the snapshot at $t/\tau_i = 5$ in panel (e). However, for the case in (b), the coalescence of multiple nuclei restricts their individual expansion due to spatial constraints, reminiscent of the middle nucleus in the former case. These insights unveil two pivotal aspects of rupture: (i) the growth rate of a nucleus is contingent upon its size and position relative to other nuclei on the film, and (ii) if two nuclei coalesce, the post-coalescence growth rate of the amalgamated nucleus mirrors that of individual nuclei, provided hindrance-free expansion persists. This is feasible only when two closely situated nuclei merge during an early stage of the film rupture process, namely before the onset of the coalescence regime. Our observations underscore that a straightforward temporal extrapolation, as discussed earlier, encounters limitations without comprehensive details regarding rupture dynamics and the spatio-temporal arrangement of the nuclei.

Figure 5c demonstrates how the number of neighbors impact the growth of a central (synthetic) nucleus surrounded by n neighbors. The initial radii of all the nuclei, $R(t = 0)$, and the initial center-to-center distance between the central and any of the neighbor nuclei were kept constant for all cases considered (the initial conditions are shown in panel g, color of the nuclei in panel g correspond to the symbol color in panel c). As n increases, the growth starts deflecting from the linear behavior. One can observe that at $n = 6$ (green circles), the growth curve reaches nearly a plateau - meaning the neighbors surround the central nucleus from all sides inducing sufficient

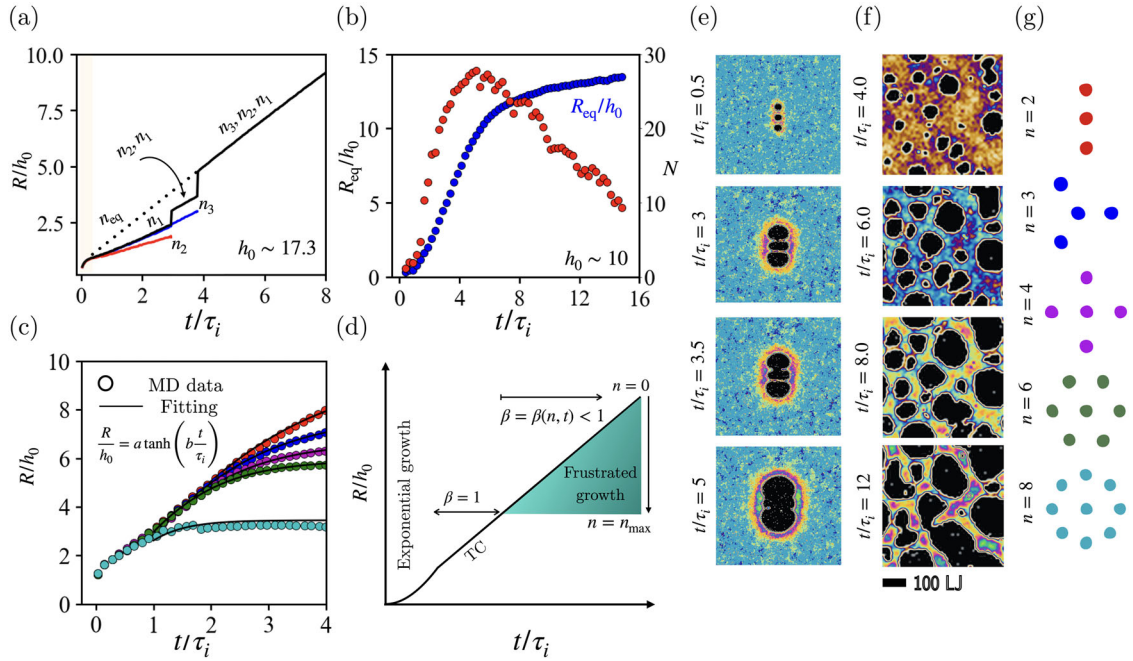

Fig. 5 | Expansion and frustration of rupture sites. a, **e** Growth of three synthetic nuclei (n_1, n_2, n_3) on a film of thickness, $h_0 \sim 17.3$. Snapshots at different instants are shown in (**e**). After a brief period of initial transients[49], each nucleus undergoes a phase of linear growth. While all nuclei initially expand at the same rate, the central nucleus experiences hindered growth due to interactions with the adjacent side nuclei, resulting in deceleration (red line). In contrast, the two side nuclei continue their growth at a consistent pace (black: n_1, blue: n_3). At $t/\tau_i \sim 3$, n_2 coalesces with n_1, continuing its growth as $n_{c,1,2}$, while n_3 maintains separate growth rate until its coalescence at $t/\tau \sim 4$. The newly merged nucleus ($n_{c,1,2,3}$) then resumes unrestrained growth. The dashed line represents the growth trajectory of an equivalent nucleus from the initiation of the linear regime. **b**, **f** Growth of the equivalent nucleus (blue circles, left y-axis) in a film of thickness $h_0 \sim 10$, where multiple holes spontaneously nucleate - as shown in (**f**). Red circles in (**b**) represent the number of nuclei, N (right y-axis). (c, g) Effect of the number of neighbors (n) on the growth of an expanding central nucleus surrounded by n neighbor nuclei as shown in (**g**), solid lines in (**c**) denote fitting to the data. **d** Schematic representation of neighbor-effect on the growth of a nucleus. Every case was independently run for at least three times with standard deviation less than 3%.

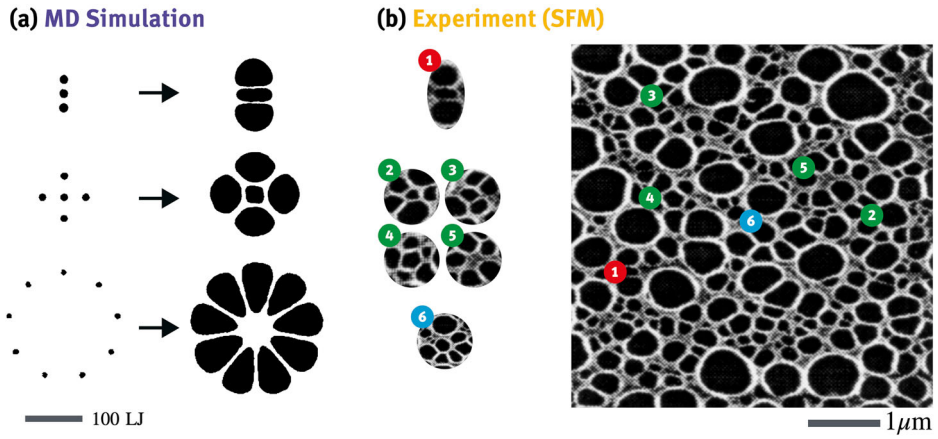

Fig. 6 | Rupture patterns. a Patterns observed in current investigations through varied synthetic perturbation. The left images depict the initial conditions, while the right images capture snapshots during the later stages of rupture. **b** The patterns observed in panel a, are compared to the those observed in the scanning force microscopy (SFM) image (adapted from panel c of Fig. 1 in Thiele et al., 1998, with permission from the authors and the publishers) of a collagen film on a solid substrate. Bars denote the scales in relevant units. Similar looking patterns in MD and experiments are marked by identical numbers.

wall effect to suffocate further growth. If n is increased beyond 6, the initial growth is shortened and the growth of the central nucleus soon ceases. The solid lines in panel (b) corresponds to fitting of the MD data to an equation of the form, $R/h_0 = a\ \tanh(bt/\tau_i)$, where a and b are fitting coefficients. An expansion of the fitting equation suggests that the frustrated growth can indeed be captured through higher order corrections to the Taylor-Culick law of retraction, i.e., $R/h_0 = c_1(R_{TC}/h_0) - \mathcal{O}(\chi^n)$, here, R_{TC} is the unrestrained radius of the nucleus at time t, and c_1 is the coefficient of the expansion whose magnitudes is governed by the frustration of growth, and $\mathcal{O}(\chi^n)$ denotes higher order terms in the expansion. The different stages of nucleus growth including the above mentioned frustrated regime is schematically presented in panel (d). The early-time exponential growth is followed by the Taylor-Culick linear growth, ($U = \beta U_{TC}$), with $\beta = 1$. Upon sufficient expansion, when a nucleus comes into close proximity of its neighbors, the growth is slowed ($\beta < 1$). The extent to which the growth is frustrated depends on the number of neighbors. As $n \to n_{max}$ (see Supplementary Note 4: Neighbor Effect on the Rupture Propagation for further details), the frustration is maximized and growth is ceased.

As time unfolds, the resulting grown-up patterns show striking similarity with patterns observed in earlier experimental studies. Figure 6 compares some of the patterns observed in the present investigation with the experimental findings by Thiele et al.[61]. The left column on panel (a) presents the initial stages of synthetic nuclei, which are allowed to evolve over time, the corresponding later stages are displayed on the right column of the

panel. Panel (b) shows similar looking patterns found through scanning force microscopy of collagen film rupturing on a solid substrate, revealing a diverse array of rupture sites with varying shapes and sizes. This coherence between our simulations and experimental observations underscores the effectiveness of MD simulations in capturing the spatio-temporal dynamics of liquid film rupture.

To summarize, the present investigation portrays the complete life cycle of a black film, delving into its inception, evolution, and ultimate fragmentation with insights into these phases. Our findings contrast the conventional understanding of rupture in pure films, revealing that the unfolding of film morphologies—commonly characterized as spinodal and nucleation dominated rupture – are broadly analogous except for their respective timescales. The highly resolved time in our investigation also discloses a 'film-pinching' phase preceding the exponential growth of rupture. A brief but discernible window of determinism, which emerges amidst the stochastic nature of rupture dynamics, indicates the liquid's inherent structure as the gateway to predicting rupture. Following the evolution of the rupture sites through exponential and linear growths, the late stage is marked by considerable frustration in growth, resulting in delayed coalescence and coarsening. In essence, our study sheds light on the intricacies of rupture dynamics, providing valuable insights into the underlying mechanisms governing this phenomenon. These not only expand our fundamental understanding of thin film behavior, but also open doors to potential applications in various scientific and technological domains.

Methods

Molecular dynamics simulations

The model films studied here are composed of single component Lennard-Jones (LJ) particles, i.e.,

$$U_{ij}(r) = 4\epsilon_{ij}\left[\left(\frac{\sigma_{ij}}{r_{ij}}\right)^{12} - \left(\frac{\sigma_{ij}}{r_{ij}}\right)^{6}\right]$$

here, U_{ij} is the potential between particle i and j located at a distance r_{ij}, and free from electrostatic interactions. The dispersion energy is described by ϵ_{ij}, and σ_{ij} is the characteristic length scale. Periodic boundary conditions are applied in all three Cartesian directions. Simulations were carried out employing the extensively validated and verified Flowmol MD code[85].

The initial simulation domain was represented by a cubic box with dimensions $L_x = 76.19$ and $L_y = L_z = 609.56$ in LJ units, translating to film dimensions approximately 207 nm wide and with a depth (h_0) of less than 5 nm. In order to reduce the computational cost in simulating the relatively large systems, a cut-off radius, $r_c = 2.5$ is used which has been proved to be sufficient in previous film rupture studies[49,86,87]. Throughout this paper, all measurements and quantities are expressed in LJ units. The central 20% of the simulation box along the x axis was assigned as the liquid phase, with a targeted density of $\rho \approx 0.7$, while the remaining region was designated as the vapor phase with a lower density of $\rho \approx 0.01$. A cohesive central liquid film, consisting of around ~ 0.4–1.8 million identical atoms, coexists harmoniously with the surrounding vapor phase at an equilibrium state. The system was allowed to equilibrate (at $T = 0.78 \pm 0.03$) to a stable liquid-vapor coexistence state. This equilibration was conducted in the canonical ensemble (NVT), utilizing a Nośe-Hoover thermostat, over a span of 50,000 time steps with a timestep size of $\Delta t = 0.005$.

The equilibrium state served as the starting point for subsequent production runs in the microcanonical (NVE) ensemble. This phase proceeds without the intervention of any thermostat or other external control mechanisms, thereby enabling the natural evolution of the system, and the emergence of nanoscale fluctuations intrinsic[27,67,86,88] to the phenomena of interest. In addition to a system's ability to evolve freely from external thermostat interference in the micro-canonical ensemble[89], this choice is further motivated by several factors. One of the most efficient thermostats, i.e., the Nose-Hoover thermostat, has been shown to alter mean square displacement and potentially disrupt time-dependent correlations in fluids[90]. In light of the uncertainties surrounding the impact of thermostats on transport properties[91], the choice of the NVE ensemble ensures that energy transformations occur naturally, thereby providing a more accurate depiction of the system's dynamics without artificial adjustments[92,93]. To explore films with different thicknesses, the dimension in the x direction was systematically varied.

Restart simulations. System states, $\Gamma(t)$, were saved at regular intervals, creating restart points which we denote as time t_0. For restarting a simulation the restart state $\Gamma(t_0)$ served as the initial condition. This ensured that multiple independent simulations restarted at t_0 from an identical initial state with a different trajectory due to the divergence of trajectories in phase space. In this rewind exercise, we restarted the simulations applying a small random nudge to all the particle velocities. To perturb the particle velocities, $\boldsymbol{v}_i$ for all particles, i were nudged as $\boldsymbol{v}_i(t_n) = \boldsymbol{v}_i(t_0) + \Delta\boldsymbol{v}_i$ to create any of n nudged trajectories, where $\Delta\boldsymbol{v}_i = C\boldsymbol{\zeta}_i$, with $C = 10^{-8}$, and $\boldsymbol{\zeta}_i$ is a random number. It was ensured that the cumulative sum of these perturbations remained zero, i.e., $\sum_{i=1}^{N}(\Delta v_i) = 0$, precluding the introduction of any net momentum into the system.

Synthetic nucleation. To initiate synthetic nucleation, we applied an external force, as in Eq. (1), to mimic the popular experimental film-puncturing procedure[81,84,94].

$$F_{\text{ext.}} = \begin{cases} F\left(1 + \mathrm{e}^{-1/r^2}\right) & r \le R_0 \\ 0 & \text{otherwise,} \end{cases} \tag{1}$$

where, R_0 is the initial radius of the hole. The forcing time was only a few hundred time-steps to confirm that a stable hole is created, and R_0 was kept sufficiently small of the order of the film thickness. Prior investigations[49] have demonstrated that this artificial nucleation process does not impact the growth dynamics of the nuclei. Readers are referred to ref. 49 for further details of the simulation.

Finite element analysis employing Cahn-Hilliard Theory

The finite element analysis for the Cahn-Hilliard theory uses a mixed formulation which recast the fourth-order equation into two coupled second-order equations. This bypasses the C^1-continuous requirement of the Galerkin method and has shown[95,96] to give comparable accuracy to the C^1-continuous methods whilst being less computationally expensive. To realize the finite element formulation, the solution of a system state is given via a interpolation function $A(\mathbf{x}) = \sum_{i=1}^{N} A_i N_i(\mathbf{x})$, where N_i is the finite-element basis, and A_i is the coefficient for each bilinear elements with the indices $i = 1, \ldots, N$. A standard rectangular mesh is used whereby the initial conditions are imported from a state of the MD simulations. The FEM package FENiCs[97] is used for the calculation and the time discretisation uses the Crank-Nicolson method. The Newton-Krylov solvers based on PETSc's SNES module is used with the discretisations in space and time solved using the general minimal residual method (GMRES). Each iteration is solved to a relative tolerance of 10^{-6}.

Data availability

Configuration files for molecular dynamics simulations are publicly available at: https://doi.org/10.5281/zenodo.12633918. Any additional data is available upon reasonable request to the corresponding author.

Code availability

Codes to reproduce the data reported in this manuscript can be found at the github public repository: https://github.com/MuhammadRRahman/Thin-Film-Rupture-NEMD.git.

Received: 12 February 2024; Accepted: 11 July 2024;
Published online: 17 July 2024

References

1. Durán-Olivencia, M. A., Gvalani, R. S., Kalliadasis, S. & Pavliotis, G. A. Instability, rupture and fluctuations in thin liquid films: theory and computations. *J. Stat. Phys.* **174**, 579–604 (2019).
2. Craster, R. V. & Matar, O. K. Dynamics and stability of thin liquid films. *Rev. Mod. Phys.* **81**, 1131 (2009).
3. Ancey, C. Plasticity and geophysical flows: a review. *J. Non-Newton. Fluid Mech.* **142**, 4–35 (2007).
4. Goldstein, R. E., Huppert, H. E., Moffatt, H. K. & Pesci, A. I. Instability of a gravity current within a soap film. *J. Fluid Mech.* **753**, R1 (2014).
5. Grotberg, J. B. Respiratory fluid mechanics and transport processes. *Annu. Rev. Biomed. Eng.* **3**, 421–457 (2001).
6. Villermaux, E. Fragmentation versus cohesion. *J. Fluid Mech.* **898**, P1 (2020).
7. Tammaro, D. et al. Flowering in bursting bubbles with viscoelastic interfaces. *Proc. Natl Acad. Sci.* **118**, e2105058118 (2021).
8. Griesser, H. J.*Thin film coatings for biomaterials and biomedical applications* (Woodhead Publishing, 2016).
9. Piegari, A. & Flory, F. *Optical thin films and coatings: From materials to applications* (Woodhead Publishing, 2018).
10. Stone, H. A., Stroock, A. D. & Ajdari, A. Engineering flows in small devices: microfluidics toward a lab-on-a-chip. *Annu. Rev. Fluid Mech.* **36**, 381–411 (2004).
11. Eijkel, J. C. & Berg, Avd Nanofluidics: what is it and what can we expect from it? *Microfluid. Nanofluidics* **1**, 249–267 (2005).
12. Scheludko, A. Sur certaines particularités des lames mousseuses. *Proc. K. Nederlandse Akad. van. Wet. B* **65**, 86–99 (1962).
13. Kashchiev, D. & Exerowa, D. Nucleation mechanism of rupture of newtonian black films. i. theory. *J. Colloid Interface Sci.* **77**, 501–511 (1980).
14. Derjaguin, B. & Prokhorov, A. On the theory of the rupture of black films. *J. Colloid Interface Sci.* **81**, 108–115 (1981).
15. Vaynblat, D., Lister, J. R. & Witelski, T. P. Rupture of thin viscous films by van der waals forces: evolution and self-similarity. *Phys. Fluids* **13**, 1130–1140 (2001).
16. Saulnier, F., Raphaël, E. & De Gennes, P.-G. Dewetting of thin-film polymers. *Phys. Rev. E* **66**, 061607 (2002).
17. Evers, L. J., Shulepov, S. Y. & Frens, G. Rupture of thin liquid films from newtonian and viscoelastic liquids. bursting behaviour of newton-black films. *Faraday Discuss.* **104**, 335–344 (1996).
18. Nikolova, A. & Exerowa, D. Rupture of common black films: experimental study. *Colloids Surf. A Physicochem. Eng. Asp.* **149**, 185–191 (1999).
19. Casteletto, V. et al. Stability of soap films: hysteresis and nucleation of black films. *Phys. Rev. Lett.* **90**, 048302 (2003).
20. Shen, Z., Sun, H., Liu, X., Liu, W. & Tang, M. Stability of newton black films under mechanical stretch–a molecular dynamics study. *Langmuir* **29**, 11300–11309 (2013).
21. Gamba, Z., Hautman, J., Shelley, J. C. & Klein, M. L. Molecular dynamics investigation of a newtonian black film. *Langmuir* **8**, 3155–3160 (1992).
22. Bresme, F. & Faraudo, J. Computer simulation studies of newton black films. *Langmuir* **20**, 5127–5137 (2004).
23. Jang, S. S. & Goddard, W. A. Structures and properties of newton black films characterized using molecular dynamics simulations. *J. Phys. Chem. B* **110**, 7992–8001 (2006).
24. Tarazona, P., Martínez, H., Chacón, E. & Bresme, F. Newton black films as wetting systems. *Phys. Rev. B* **85**, 085402 (2012).
25. De Vries, A. Foam stability: Part v. mechanism of film rupture. *Recl. des. Trav. Chim. des. Pays-Bas* **77**, 441–461 (1958).
26. Vrij, A. Possible mechanism for the spontaneous rupture of thin, free liquid films. *Discuss. Faraday Soc.* **42**, 23–33 (1966).
27. Zhang, Y., Sprittles, J. E. & Lockerby, D. A. Molecular simulation of thin liquid films: thermal fluctuations and instability. *Phys. Rev. E* **100**, 023108 (2019).
28. Langevin, D. On the rupture of thin films made from aqueous surfactant solutions. *Adv. Colloid Interface Sci.* **275**, 102075 (2020).
29. Yaminsky, V. V., Ohnishi, S., Vogler, E. A. & Horn, R. G. Stability of aqueous films between bubbles. part 2. effects of trace impurities and evaporation. *Langmuir* **26**, 8075–8080 (2010).
30. Anderson, A. M., Brush, L. N. & Davis, S. H. Foam mechanics: spontaneous rupture of thinning liquid films with plateau borders. *J. Fluid Mech.* **658**, 63–88 (2010).
31. Prévost, M. & Gallez, D. Nonlinear rupture of thin free liquid films. *J. Chem. Phys.* **84**, 4043–4048 (1986).
32. Erneux, T. & Davis, S. H. Nonlinear rupture of free films. *Phys. Fluids A Fluid Dyn.* **5**, 1117–1122 (1993).
33. Williams, M. B. & Davis, S. H. Nonlinear theory of film rupture. *J. Colloid Interface Sci.* **90**, 220–228 (1982).
34. Sheludko, A. Thin liquid films. *Adv. Colloid Interface Sci.* **1**, 391–464 (1967).
35. Knutton, S. Studies of membrane fusion.: Iii. fusion of erythrocytes with polyethylene glycol. *J. Cell Sci.* **36**, 61–72 (1979).
36. Forrest, J., Dalnoki-Veress, K., Stevens, J. & Dutcher, J. Effect of free surfaces on the glass transition temperature of thin polymer films. *Phys. Rev. Lett.* **77**, 2002 (1996).
37. Ge, S. et al. Shear modulation force microscopy study of near surface glass transition temperatures. *Phys. Rev. Lett.* **85**, 2340 (2000).
38. Shiri, R., Schmeller, L., Peschka, D., Seemann, R. & Wagner, B. Impact of noise on spinodal dewetting of liquid-liquid films. *Commun. Phys.* **6**, 109 (2023).
39. Sharma, A., Mittal, J. & Verma, R. Instability and dewetting of thin films induced by density variations. *Langmuir* **18**, 10213–10220 (2002).
40. Morariu, M., Schäffer, E. & Steiner, U. Capillary instabilities by fluctuation induced forces. *Eur. Phys. J. E* **12**, 375–381 (2003).
41. Israelachvili, J. N. Surface forces. In *The Handbook of Surface Imaging and Visualization*, 793–816 (CRC Press, 2022).
42. Chatzigiannakis, E. & Vermant, J. Breakup of thin liquid films: from stochastic to deterministic. *Phys. Rev. Lett.* **125**, 158001 (2020).
43. Schebarchov, D., Lefèvre, B., Somerville, W. & Hendy, S. Filling a nanoporous substrate by dewetting of thin films. *Nanoscale* **5**, 1949–1954 (2013).
44. Nguyen, T. D., Carrillo, J.-M. Y., Matheson, M. A. & Brown, W. M. Rupture mechanism of liquid crystal thin films realized by large-scale molecular simulations. *Nanoscale* **6**, 3083–3096 (2014).
45. Langevin, D. Aqueous foams and foam films stabilised by surfactants. gravity-free studies. *Comptes Rendus Méc.* **345**, 47–55 (2017).
46. Manikantan, H. & Squires, T. M. Surfactant dynamics: hidden variables controlling fluid flows. *J. Fluid Mech.* **892**, P1 (2020).
47. Saulnier, L. et al. A study of generation and rupture of soap films. *Soft Matter* **10**, 2899–2906 (2014).
48. de Gennes, P.-G. Some remarks on coalescence in emulsions or foams. *Chem. Eng. Sci.* **56**, 5449–5450 (2001).
49. Rahman, M. R. et al. Non-equilibrium molecular simulations of thin film rupture. *J. Chem. Phys.* **158**, 151104 (2023).
50. Taylor, G. I. & Michael, D. H. On making holes in a sheet of fluid. *J. Fluid Mech.* **58**, 625–639 (1973).
51. Culick, F. E. C. Comments on a ruptured soap film. *J. Appl. Phys.* **31**, 1128–1129 (1960).
52. McEntee, W. R. & Mysels, K. J. Bursting of soap films. I. An experimental study. *J. Phys. Chem.* **73**, 3018–3028 (1969).
53. Xie, R., Karim, A., Douglas, J. F., Han, C. C. & Weiss, R. A. Spinodal dewetting of thin polymer films. *Phys. Rev. Lett.* **81**, 1251 (1998).
54. Higgins, A. M. & Jones, R. A. Anisotropic spinodal dewetting as a route to self-assembly of patterned surfaces. *Nature* **404**, 476–478 (2000).
55. Thiele, U., Velarde, M. G. & Neuffer, K. Dewetting: film rupture by nucleation in the spinodal regime. *Phys. Rev. Lett.* **87**, 016104 (2001).
56. Becker, J. et al. Complex dewetting scenarios captured by thin-film models. *Nat. Mater.* **2**, 59–63 (2003).

57. Novick-Cohen, A. The nonlinear cahn-hilliard equation: transition from spinodal decomposition to nucleation behavior. *J. Stat. Phys.* **38**, 707–723 (1985).
58. Bestehorn, M. & Neuffer, K. Surface patterns of laterally extended thin liquid films in three dimensions. *Phys. Rev. Lett.* **87**, 046101 (2001).
59. Reiter, G. Dewetting as a probe of polymer mobility in thin films. *Macromolecules* **27**, 3046–3052 (1994).
60. Stange, T., Evans, D. & Hendrickson, W. Nucleation and growth of defects leading to dewetting of thin polymer films. *Langmuir* **13**, 4459–4465 (1997).
61. Thiele, U., Mertig, M. & Pompe, W. Dewetting of an evaporating thin liquid film: Heterogeneous nucleation and surface instability. *Phys. Rev. Lett.* **80**, 2869 (1998).
62. Bischof, J., Scherer, D., Herminghaus, S. & Leiderer, P. Dewetting modes of thin metallic films: nucleation of holes and spinodal dewetting. *Phys. Rev. Lett.* **77**, 1536 (1996).
63. Herminghaus, S. et al. Spinodal dewetting in liquid crystal and liquid metal films. *Science* **282**, 916–919 (1998).
64. Jacobs, K., Herminghaus, S. & Mecke, K. R. Thin liquid polymer films rupture via defects. *Langmuir* **14**, 965–969 (1998).
65. Seemann, R., Herminghaus, S. & Jacobs, K. Dewetting patterns and molecular forces: a reconciliation. *Phys. Rev. Lett.* **86**, 5534 (2001).
66. Zhao, C., Liu, J., Lockerby, D. A. & Sprittles, J. E. Fluctuation-driven dynamics in nanoscale thin-film flows: physical insights from numerical investigations. *Phys. Rev. Fluids* **7**, 024203 (2022).
67. Sprittles, J. E., Liu, J., Lockerby, D. A. & Grafke, T. Rogue nanowaves: a route to film rupture. *Phys. Rev. Fluids* **8**, L092001 (2023).
68. Dhaliwal, V. et al. Instability and rupture of sheared viscous liquid nanofilms. *Phys. Rev. Fluids* **9**, 024201 (2024).
69. Stillinger, F. H. & Weber, T. A. Hidden structure in liquids. *Phys. Rev. A* **25**, 978 (1982).
70. Nusse, H. E., Yorke, J. A. & Kostelich, E. J. In *Dynamics: Numerical Explorations. Applied Mathematical Sciences*, **101** 269–314 (Springer, 1994).
71. Bagchi, B. *Water in biological and chemical processes: from structure and dynamics to function* (Cambridge University Press, 2013).
72. Ball, P. The hidden structure of liquids. *Nat. Mater.* **13**, 758–759 (2014).
73. Gebauer, D., Raiteri, P., Gale, J. D. & Cölfen, H. On classical and non-classical views on nucleation. *Am. J. Sci.* **318**, 969–988 (2018).
74. La Nave, E., Sastry, S. & Sciortino, F. Relation between local diffusivity and local inherent structures in the kob-andersen lennard-jones model. *Phys. Rev. E* **74**, 050501 (2006).
75. Vrij, A. & Overbeek, J. T. G. Rupture of thin liquid films due to spontaneous fluctuations in thickness. *J. Am. Chem. Soc.* **90**, 3074–3078 (1968).
76. Ruckenstein, E. & Jain, R. K. Spontaneous rupture of thin liquid films. *J. Chem. Soc.* **70**, 132–147 (1974).
77. Moreno-Boza, D., Martínez-Calvo, A. & Sevilla, A. Stokes theory of thin-film rupture. *Phys. Rev. Fluids* **5**, 014002 (2020).
78. Taylor, G. The dynamics of thin sheets of fluid iii. disintegration of fluid sheets. *Proc. R. Soc. Lond. Ser. A* **253**, 313–321 (1959).
79. Frankel, S. & Mysels, K. J. Bursting of soap films. II. Theoretical considerations. *J. Phys. Chem.* **73**, 3028–3038 (1969).
80. Keller, J. B. Breaking of liquid films and threads. *Phys. Fluids* **26**, 3451–3453 (1983).
81. Savva, N. & Bush, J. W. Viscous sheet retraction. *J. Fluid Mech.* **626**, 211–240 (2009).
82. Sünderhauf, G., Raszillier, H. & Durst, F. The retraction of the edge of a planar liquid sheet. *Phys. Fluids* **14**, 198–208 (2002).
83. Deka, H. & Pierson, J.-L. Revisiting the taylor-culick approximation. ii. retraction of a viscous sheet. *Phys. Rev. Fluids* **5**, 093603 (2020).
84. Bird, J. C., De Ruiter, R., Courbin, L. & Stone, H. A. Daughter bubble cascades produced by folding of ruptured thin films. *Nature* **465**, 759–762 (2010).
85. Smith, E. On the coupling of molecular dynamics to continuum computational fluid dynamics, PhD thesis, (Imperial College London, 2013).
86. Nguyen, T. D., Fuentes-Cabrera, M., Fowlkes, J. D. & Rack, P. D. Coexistence of spinodal instability and thermal nucleation in thin-film rupture: Insights from molecular levels. *Phys. Rev. E* **89**, 032403 (2014).
87. Koplik, J. & Banavar, J. R. Molecular simulations of dewetting. *Phys. Rev. Lett.* **84**, 4401 (2000).
88. Kadau, K. et al. Nanohydrodynamics simulations: an atomistic view of the rayleigh–taylor instability. *Proc. Natl Acad. Sci.* **101**, 5851–5855 (2004).
89. Hammonds, K. & Heyes, D. Shadow hamiltonian in classical nve molecular dynamics simulations: a path to long time stability. *J. Chem. Phys.* **152**, 024114 (2020).
90. Frenkel, D. & Smit, B. *Understanding molecular simulation: from algorithms to applications* (Elsevier, 2023).
91. Dysthe, D., Fuchs, A. & Rousseau, B. Fluid transport properties by equilibrium molecular dynamics. i. methodology at extreme fluid states. *J. Chem. Phys.* **110**, 4047–4059 (1999).
92. Rapaport, D. C. *The art of molecular dynamics simulation* (Cambridge University Press, 2004).
93. Allen, M. P. & Tildesley, D. J. *Computer simulation of liquids* (Oxford University Press, 2017).
94. Oratis, A. T., Bush, J. W., Stone, H. A. & Bird, J. C. A new wrinkle on liquid sheets: turning the mechanism of viscous bubble collapse upside down. *Science* **369**, 685–688 (2020).
95. Zhang, L. et al. A quantitative comparison between c0 and c1 elements for solving the cahn-hilliard equation. *J. Comput. Phys.* **236**, 74–80 (2013).
96. Kaessmair, S. & Steinmann, P. Comparative computational analysis of the Cahn-Hilliard equation with emphasis on C1-continuous methods. *J. Comput. Phys.* **322**, 783–803 (2016).
97. Alnæs, M. S. et al. The FEniCS Project Version 1.5. *Arch. Numer. Softw.* **3**, 9–23 (2015).
98. Dolganov, P., Shuravin, N. & Dolganov, V. Coalescence of holes in two-dimensional free-standing smectic films. *Phys. Rev. E* **101**, 052701 (2020).

Acknowledgements

M.R.R. thanks Shell, and the Beit Fellowship for Scientific Research for PhD funding. L.S. thanks the Engineering and Physical Sciences Research Council (EPSRC) for a Postdoctoral Fellowship (EP/V005073/1). J.P.E. was supported by the Royal Academy of Engineering (RAEng) through their Research Fellowships scheme. D.D. acknowledges a Shell/RAEng Research Chair in Complex Engineering Interfaces, and the EPSRC for an Established Career Fellowship (EP/N025954/1). M.R.R. thanks Prof. Uwe Thiele for valuable insights.

Author contributions

D.D., E.R.S., L.S., D.M.H. and J.P.E. conceptualized and supervised the project. D.D. and L.S. secured funding. M.R.R. developed the methodology, conducted the simulations, and analyzed the results with contributions from E.R.S. and L.S. M.R.R. drafted the manuscript with inputs from L.S. All authors contributed to result interpretation and manuscript review.

Competing interests
The authors declare no competing interests.

Additional information
Supplementary information The online version contains supplementary material available at https://doi.org/10.1038/s42005-024-01745-z.

Correspondence and requests for materials should be addressed to Muhammad Rizwanur Rahman.

Peer review information *Communications Physics* thanks the anonymous reviewers for their contribution to the peer review of this work. A peer review file is available.